The Deep Interior Downwelling, the Veronis Effect, and Mesoscale Tracer Transport Parameterizations in an OGCM

ALBAN LAZAR, GURVAN MADEC, AND PASCALE DELECLUSE

Laboratoire d'Océanographie Dynamique et de Climatologie, Unité Mixte de Recherche CNRS-ORSTOM-UPMC, Universtité Pierre et Marie Curie, Paris, France

(Manuscript received 1 May 1998, in final form 29 January 1999)

ABSTRACT

Numerous numerical simulations of basin-scale ocean circulation display a vast interior downwelling and a companion intense western boundary layer upwelling at midlatitude below the thermocline. These features, related to the so-called Veronis effect, are poorly rationalized and depart strongly from the classical vision of the deep circulation where upwelling is considered to occur in the interior. Furthermore, they significantly alter results of ocean general circulation models (OGCMs) using horizontal Laplacian diffusion. Recently, some studies showed that the parameterization for mesoscale eddy effects formulated by Gent and McWilliams allows integral quantities like the streamfunction and meridional heat transport to be free of these undesired effects. In this paper, an idealized OGCM is used to validate an analytical rationalization of the processes at work and help understand the physics.

The results show that the features associated with the Veronis effect can be related quantitatively to three different width scales that characterize the baroclinic structure of the deep western boundary current. In addition, since one of these scales may be smaller than the Munk barotropic layer, usually considered to determine the minimum resolution and horizontal viscosity for numerical models, the authors recommend that it be taken into account. Regarding the introduction of the new parameterization, diagnostics in terms of heat balances underline some interesting similarities between local heat fluxes by eddy-induced velocities and horizontal diffusion at low and midlatitudes when a common large diffusivity (here 2000 $m^2\ s^{-1}$) is used. The near-quasigeostrophic character of the flow explains these results. As a consequence, the response of the Eulerian-mean circulation is locally similar for runs using either of the two parameterizations. However, it is shown that the advective nature of the eddy-induced heat fluxes results in a very different effective circulation, which is the one felt by tracers.

1. Introduction

In a pioneering paper on circulation modeling, Holland (1971) discovered a surprising pattern below the thermocline using an idealized OGCM. In contrast with the Stommel and Arons (1960, hereafter SA) theory, a large part of the midlatitude interior ocean below the thermocline was characterized by downwelling instead of the expected upwelling. This pattern was associated with an intense western boundary layer (WBL) upwelling. A few years later, Veronis (1975) presented an analysis of this run showing that the cold upwelling was actually balancing a strong diapycnal flux of heat from the interior caused by the horizontal diffusion term, due to the steeply sloping isotherms of the deep western boundary current (DWBC). He suggested that, in addition to the deep-water formation region, more downwelling was necessary to compensate the mass loss associated with the WBL upwelling and that this mechanism could explain the anomalous negative vertical velocities in the interior. Whereas the results of Gough and Lin (1995) supported the continuity argument, no evidence was found to explain the location of the downwelling region and a satisfying rationalization was still missing. Since then, the Veronis upwelling/downwelling system appeared to be a ubiquitous and insufficiently understood feature of idealized OGCMs, especially those using horizontal diffusivity of more than about 1000 $m^2\ s^{-1}$ (e.g., Bryan 1987; Cummins et al. 1990; Gough and Lin 1995). At the same time, models with realistic geometry were also undergoing an intense WBL upwelling, related to the same effect, that was considered to be responsible for wrong tracer distributions (Toggweiler et al. 1989) and anomalously weak northward heat transport (Böning et al. 1995).

Considered an artifact of an insufficiently accurate representation of eddy effects on tracers, the phenomenon was expected to disappear with the use of the isopycnal mixing tensor provided by Redi (1982), but the need of a background horizontal diffusion (for numerical stability) did not allow the complete elimination

Corresponding author address: Dr. Alban Lazar, Laboratory for Hydrospheric Processes, Code 970, Goddard Space Flight Center NASA, Greenbelt, MD 20771.

of the undesired effects (e.g., Cummins et al. 1990; Gough and Welch 1994). Meanwhile, the introduction of a new parameterization for eddy-induced transport by Gent and McWilliams (1990, hereafter GM) avoided the use of any horizontal diffusion term and led to a dramatic reduction of the main biases attributed to the Veronis upwelling/downwelling system (Böning et al. 1995; Danabasoglu and McWilliams 1995; Weaver and Eby 1997). In these studies, no explanation was given for the mechanisms responsible for the disappearance of the anomalous patterns, and the physics of the Veronis effect remained obscure.

Using a reduced gravity model of an idealized deep ocean basin, Masuda and Uehara (1992, MU) also experienced the Veronis effect. By determining the various baroclinic zonal scales of their DWBC, following similar studies with a continuously stratified analytical model by Pedlosky (1969) and Warren (1976), they proposed a promising rationalization of the phenomenon. In their study, these authors suggested how analytically determined length scales and associated vorticity regimes could give the size and the location of the interior downwelling as well as the nature of the WBL dynamics as a function of mixing parameters (horizontal viscosity and diffusivity) and the stratification of the fluid.

Our study is aimed at verifying the MU suggestion in an idealized OGCM and to develop a physical understanding of the Veronis effect beyond the mathematical rationalization. Only the middepth regimes (depth 1000–3000 m) is analyzed here because other types of circulation may develop in the abyss (depth 3000–5000 m); they will be addressed in a separate paper. We also propose an analysis of the improvement process resulting from the use of the GM parameterization and provide general insights into the behavior of this turbulent closure scheme. Section 2 describes the model and the experiments. The analytical rationalization proposed by MU (for a two-layer fluid) is presented in section 3 in a continuously stratified fluid context. Section 4 presents diagnostics in terms of vorticity and heat balances that allow a precise comparison of the theory to the numerical results obtained with both Laplacian diffusion and eddy-induced transport representation of the mesoscale eddy effects. A more ''physical'' interpretation of the results is presented in section 5, and section 6 presents our conclusions.

2. Numerical model and experiments

a. Model geometry and forcing

The idealized basin model used here is based on ''OPA,'' the OGCM developed at the Laboratoire d'Océanographie Dynamique et de Climatologie and described, for example, in Madec and Imbard (1996). It uses primitive equations in spherical coordinates. The domain is a 40° wide sector of the sphere extending from 60°N to the equator, where symmetrical conditions are imposed, and has a constant depth of 5000 m. Such a basin geometry is adequate to simulate idealized large-scale circulation patterns and is comparable to previous process studies (e.g., Holland 1971; Cummins et al. 1990; Suginohara and Aoki 1991). It has a uniform 1° horizontal resolution and there are 30 levels with vertical spacings ranging from 10 m at the surface to roughly 500 m below 1000-m depth as indicated in Table 1 (Madec and Imbard 1996).

TABLE 1. Vertical spacing used in the experiments and lateral diffusivity prescribed in expt HrN ($m^2\ s^{-1}$).

Model level	Depth of grid point (m)	Thickness of grid box (m)	K_L for expt HrN
1	5	10	2000
2	15	10	1987
3	25	10	1974
4	35	10	1961
5	45	10	1947
6	55	10	1932
7	65	10	1916
8	75.1	10.1	1900
9	85.2	10.1	1883
10	95.5	10.3	1865
11	105.9	10.6	1846
12	116.9	11.2	1825
13	128.7	12.4	1803
14	142.2	14.7	1777
15	158.9	19.2	1744
16	181.9	27.6	1700
17	216.65	43.2	1631
18	272.48	70.8	1516
19	364.30	116.1	1315
20	511.5	181.5	1004
21	732.2	261	689
22	1033.2	339.3	536
23	1405.7	402.2	503
24	1830.8	444.8	500
25	2289.7	470.5	500
26	2768.2	484.9	500
27	3257.4	492.7	500
28	3752.4	496.7	500
29	4250.4	498.9	500
30	4749.9	500	500

The forms of the heat and freshwater fluxes applied at the surface are

$$Q = Q_{\text{obs}} + \lambda(T_{\text{obs}} - T) \tag{2.1}$$

$$E - P = (E - P)_{\text{obs}} + \mu(S_{\text{obs}} - S), \tag{2.2}$$

where T is the temperature and S the salinity of the upper layer; Q_{obs}, $(E - P)_{\text{obs}}$, T_{obs}, and S_{obs} are constant in time and longitude and they are issued from annually and zonally averaged climatologies of the Southern Hemisphere (Southern Hemisphere forcing has been chosen because it insures the occurrence of deep-water formation at the polar boundary of our model. The zonal averaging of the Northern Hemisphere data would include the forcing associated with the North Pacific high buoyancy region and would therefore tend to lessen the deep-water formation rate). The freshwater flux $(E - P)_{\text{obs}}$ is computed from the Bryan and Oort (1984) atlas,

the net heat flux Q_{obs}, and the penetrating solar radiation from the Esbensen and Kushnir (1981) atlas, and the temperature T_{obs} and salinity S_{obs} from the Levitus (1982) climatology. The coefficient λ is associated to the feedback of the SST on the atmospheric heat flux and is equal to 20 W m^{-2} K^{-1}. The coefficient μ has little physical justification because there is no such direct feedback of SSS on precipitation and evaporation; however, we chose to use this restoring term with a value resulting in the same restoration timescale as for Q (around 24 days over the first 10 m). A penetrating solar radiation scheme is used. The wind stress forcing is computed from a Southern Hemisphere annual and zonal average of the Hellerman and Rosenstein (1983) atlas. The (in situ) density is calculated using the Jackett and McDougall (1995) formulation.

b. Formulation of the subgrid-scale physics

In several experiments, an order 1.5 turbulent closure scheme (Blanke and Delecluse 1993) is used to calculate the vertical viscosity A_V and diffusivity K_V. This scheme simulates convection by giving large mixing coefficients. In regions where the turbulent kinetic energy reaches its minimum fixed value of 0.5×10^{-6} m^2 s^{-2} (i.e., roughly below the mixed layer), this scheme is equivalent to the Gargett (1984) formulation. Therefore, in the corresponding experiments for the regions assessed in this study, namely, the deep ocean below the thermocline at low and midlatitudes, the formulation is very close to the one used by Cummins et al. (1990) for their vertical diffusion coefficient and reduces to

$$K_V = A_V = a_0 N^{-1}, \tag{2.3}$$

where a_0 is set to 0.7×10^{-7} m^2 s^{-2} and the Brunt–Väisälä frequency N is given by

$$N = \left(-\frac{g}{\rho_0} \rho_z \right)^{1/2}, \tag{2.4}$$

with ρ_0 a reference density and ρ_z the vertical gradient of locally referenced potential density. The minimum values for K_V and A_V are specified to be 10^{-5} and 10^{-4} m^2 s^{-1}, respectively (values attained at low latitudes beneath the mixed layer). The resulting vertical diffusivity and viscosity fields vary slightly in the different experiments using this fluid-dependent formulation, but they all exhibit the following gross depth-profile features: a value increasing slowly from 10^{-4} at the base of the thermocline (near 1000-m depth) to 3×10^{-4} at middepth (near 2500 m) and rising faster in the abyss up to roughly 10^{-3} m^2 s^{-1} near the bottom (Fig. 1). For a discussion of the physics of a comparable profile, see Cummins et al. (1990). The minimum value of K_V is realistic compared with measurements by Ledwell et al. (1999) and the values reached at middepth are in agreement with some indirect estimates of $O(10^{-4})$ m^2 s^{-1} (e.g., Munk 1966; Gill 1973); regarding the deepest values, their order of magnitude is probably more relevant to rough topography than to flat bottom (see, e.g., the review by Toole 1998) but, as developed later in this paper, experiment HC shows that our results are not qualitatively affected by the use of smaller vertical diffusivities below the thermocline (since we are concerned with middepth circulation).

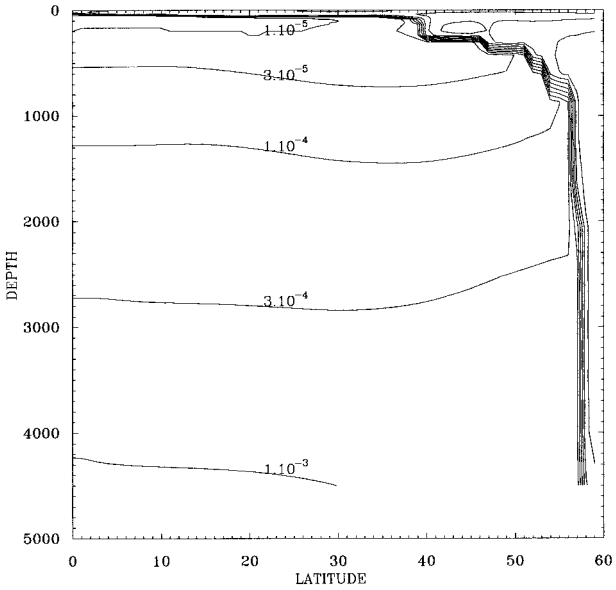

FIG. 1. Meridional section of vertical diffusivity (in m^2 s^{-1} at 20°E) displaying values characteristic of latitudes below 40°N and depth greater than 1000 m in experiments using the 1.5-order turbulent closure scheme.

The conservation equation for a tracer τ (here potential temperature or salinity) obtained with the horizontal diffusion parameterization is

$$\tau_t + \mathbf{U}_h \cdot \boldsymbol{\nabla}_h \tau + w\tau_z = K_L \Delta_h \tau + (K_V \tau_z)_z, \tag{2.5}$$

where $\boldsymbol{\nabla}_h$ and Δ_h are the gradient and Laplacian operators in the horizontal and K_L is the lateral (horizontal) diffusivity. Advection in this case is by the Eulerian-mean velocity ($\mathbf{U}_h$, w).

In the experiments where mesoscale eddy effects are parameterized by isopycnal mixing (Redi 1982) and the GM parameterization, the equation for tracer evolution is then

$$\tau_t + (\mathbf{U}_h + \mathbf{U}_h^*) \cdot \boldsymbol{\nabla}_h \tau + (w + w^*)\tau_z = \rho_z \boldsymbol{\nabla}_n \cdot \left(\frac{K_L}{\rho_z} \boldsymbol{\nabla}_n \tau \right) + (K_V \tau_z)_z. \tag{2.6}$$

Here the first term on the rhs is the standard term for isopycnal diffusion and $\boldsymbol{\nabla}_n$ is the two-dimensional gradient operator applied along neutral density surfaces. We used the isopycnal diffusion scheme proposed by Cox (Cox 1987; GM). ($\mathbf{U}_h^*$, w^*) is the eddy-induced transport velocity and is given by (GM; Gent et al. 1995)

$$\mathbf{U}_h^* = -(K_L \mathbf{S})_z, \qquad w^* = \boldsymbol{\nabla}_h \cdot (K_L \mathbf{S}), \tag{2.7}$$

TABLE 2. Summary of numerical experiments. Mixing coefficients are in $m^2\ s^{-1}$.

Exp	A_H	A_V	K_L	K_V	Diffusive tensor orientation
HC	4×10^4	10^{-4}	2000	10^{-5}	Geopotential
HN	4×10^4	1.5 closure	2000	1.5 closure	Geopotential
HrN	4×10^4	1.5 closure	2000/500	1.5 closure	Geopotential
GMN	4×10^4	1.5 closure	2000	1.5 closure	Isopycnic
GMrN	4×10^4	1.5 closure	500	1.5 closure	Isopycnic

where $\mathbf{S}(S_x, S_y)$ is the two-dimensional slope vector (along which isopycnal diffusion is applied)

$$\mathbf{S} = -\frac{\boldsymbol{\nabla}_h \rho}{\rho_z}, \tag{2.8}$$

with ρ the locally referenced potential density. Note that we chose to use the same coefficient K_L for horizontal, isopycnal, and thickness diffusivities. This coefficient may be seen as a generic lateral subgrid-scale mixing representation. This slope is required to be less than 1: 100 everywhere. Such a condition will lead to diapycnal diffusive heat (salt) fluxes in regions where isotherm (isohaline) slopes are larger than this value (Gerdes et al. 1991; Danabasoglu and McWilliams 1995; Gough 1997) and may therefore produce a small Veronis effect (compared to horizontal mixing). To ensure that the eddy-induced transport vanishes at the boundaries, the slope vector is set to a constant null value there (for additional information on the model closure, see, e.g., Guilyardi et al. 1999, submitted to *J. Phys. Oceanogr.*). One can see from (2.7) that the transition from the slope values in the ocean interior to the imposed null value at the boundaries can be associated with strong eddy-induced velocities. This is a well-known problem in the formulation of eddy-induced velocities that some authors chose to solve by smoothly tapering K_L to zero either near side boundaries (McWilliams and Gent 1994) or when $|\mathbf{S}|$ increases above a critical value (e.g., Danabasoglu and McWilliams 1995; Robitaille and Weaver 1995). These methods introduce a spatial structure in K_L, which realism is delicate to evaluate in primitive equation ocean models (see Treguier et al. 1997). In this study we decided to use a uniform value for K_L: this choice on the vertical has the advantage of allowing potential vorticity and tracers to mix in a similar way (Gent et al. 1995; Treguier et al. 1997). Consequently, it is necessary to taper $\mathbf{S}$ near the upper boundary (we imposed a linear decrease to zero between 70 m and the surface). That eddies ''feel'' the surface in the real ocean accounts for this flattening of neutral surfaces. A comparable method is used by Hirst and McDougall (1996), who imposed a vertical profile of maximum allowable slope $|\mathbf{S}|$.

c. Details of the experiments

The five experiments performed in this study are listed Table 2. All experiments use horizontal Laplacian mixing with a viscosity A_H of $4 \times 10^4\ m^2\ s^{-1}$. The reference experiment HN uses Laplacian diffusion with K_L equal to $2 \times 10^3\ m^2\ s^{-1}$, while the vertical coefficients are calculated using the 1.5 order turbulent closure scheme. HC uses the same K_L, but A_V and K_V are set to small constant values equal to 10^{-4} and $10^{-5}\ m^2\ s^{-1}$, respectively (with $A_V = K_V = 1\ m^2\ s^{-1}$ in case of unstable stratification). HrN has the same vertical physics as HN, but K_L is a function of depth decreasing to a relatively small value of $500\ m^2\ s^{-1}$, reached at a depth below 1500 m (Table 1). This depth dependence mimics the order of magnitude reduction in lateral diffusivity observed in some data (Olbers et al. 1985). The last two experiments, GMN and GMrN, are similar to HN and HrN, respectively, except that they parameterize the lateral subgrid-scale processes differently. Both use the 1.5 turbulent closure with the same parameters. GMN uses the GM formulation with $K_L = 2 \times 10^3\ m^2\ s^{-1}$. In GMrN, K_L is equal to $500\ m^2\ s^{-1}$. Hence, GMrN and HrN have the same K_L only below 1000 m.

All experiments were run to quasi equilibrium using the acceleration technique of Bryan (1984) with a tracer time step of one day in the upper ocean, increasing to three days at the deepest model level and a five-minute uniform time step for momentum. Then we performed approximately 50 years of synchronous integration (equal and uniform 2-h time step for tracer and momentum) to reach an equilibrium state with nondistorted physics. Experiments were considered equilibrated when the level averages of the potential temperature and the salinity trends dropped below 0.1°C and 0.01 psu per millennium.

3. Analytical model results

Following Edwards and Pedlosky (1995), for example, we consider a continuously stratified model of a deep oceanic basin with rectangular geometry where motion is considered to be hydrostatic, incompressible, and geostrophic along the x axis and semigeostrophic along the y axis. Each variable is written as the sum of an interior solution (governed by inviscid linear dynamics and a vertical advection/diffusion density balance) and a boundary layer correction function. Consider the case where vertical diffusion is small compared to horizontal diffusion. Then the main density balance is between vertical advection and horizontal diffusion and the equations of the correction function are

$$f\rho_0 v = p_x \tag{3.1}$$

$$f\rho_0 u = -p_y + A_H v_{xx} \tag{3.2}$$

$$u_x + v_y + w_z = 0 \tag{3.3}$$

$$\rho g = -p_z \tag{3.4}$$

$$w\frac{\rho_0}{g}N^2 = K_L\rho_{xx}, \tag{3.5}$$

where f is the (variable) Coriolis parameter, ρ_0 is a constant density typical of the deep ocean, p is the pressure anomaly that drives the anomalous motion (u, v, w), and ρ is the density anomaly related to the motion; N^2 is a constant defined by $N^2 = -g\overline{\rho}_z/\rho_0$ in which $\overline{\rho}$ is the full background density field. The equation for p is then

$$p_{xxxx} + \frac{f^2K_L}{N^2A_H}p_{xxzz} - \frac{\beta}{A_H}p_x = 0. \tag{3.6}$$

The pressure is expanded in normal modes in the vertical

$$p = \sum_{m=0}^{\infty} P_m(x)G_m(z), \tag{3.7}$$

where the upper and lower boundary conditions (the density anomaly is zero at the surface and the bottom) giving

$$G_m = \cos\left(\frac{m\pi z}{D}\right), \tag{3.8}$$

with D the depth of the basin. Multiplying (3.6) by G_m and integrating over D leads to

$$(P_m)_{xxxx} - \frac{K_L}{A_HR^2}(P_m)_{xx} - \frac{\beta}{A_H}(P_m)_x = 0, \tag{3.9}$$

where $R = ND/fm\pi$ is a Rossby radius of deformation for the mth baroclinic mode. Following the procedure used by MU to solve a comparable equation in their reduced-gravity model, we consider that solutions of Eq. (3.9) of boundary layer character are linear combinations of functions of the form $e^{\alpha x}$, with α being complex. Then α is the inverse zonal scale of the pressure correction function and the cubic equation it satisfies is (omitting the zero root)

$$\alpha^3 - \frac{K_L}{A_HR^2}\alpha - \left(\frac{\beta}{A_H}\right) = 0 \tag{3.10}$$

with β the y derivative of f. Here we are only interested in the western boundary layer solutions, which dominate the DWBC structure, and therefore consider only the roots of (3.10) with a negative real part. Note that the barotropic solution ($m = 0$) is that of Munk (1950). For the first baroclinic mode ($m = 1$), two different regimes emerge (following the criterion for determining the solution of a cubic equation using the method of Cardan). The first regime occurs when

$$\sqrt{\frac{3A_H}{K_L}}R > \left(\frac{2A_H}{\beta}\right)^{1/3}, \tag{3.11}$$

and only the two conjugate complex roots of (3.10) have a negative real part giving the zonal scale ($\equiv\{\mathrm{Re}[\alpha]\}^{-1}$):

$$L_M = \left(\frac{A_H}{\beta}\right)^{1/3} \tag{3.12}$$

if

$$\left(\frac{A_H}{\beta}\right)^{1/3} \ll \sqrt{\frac{A_H}{K_L}}R. \tag{3.13}$$

This solution corresponds to a balance between the first and third terms of (3.10); it is called the ''Carrier–Munk'' scale by Blumsack (1973). Like the Munk barotropic layer, this baroclinic layer has a vertical vorticity equilibrium dominated by planetary advection and horizontal diffusion ($\beta v = A_H\Delta\zeta$). The second regime occurs when

$$\sqrt{\frac{3A_H}{K_L}}R < \left(\frac{2A_H}{\beta}\right)^{1/3}, \tag{3.14}$$

and there are two negative real roots that correspond to two zonal scales ($\equiv\alpha^{-1}$):

$$L_H = \sqrt{\frac{A_H}{K_L}}R \tag{3.15}$$

$$L_W = \frac{K_L}{\beta R^2} \tag{3.16}$$

if, instead,

$$\left(\frac{A_H}{\beta}\right)^{1/3} \gg \sqrt{\frac{A_H}{K_L}}R. \tag{3.17}$$

The solution L_H corresponds to an equilibrium between the first and second terms of (3.10) (i.e., horizontal vorticity diffusion against vortex stretching: $A_H\Delta\zeta = -fw_z$, and the solution L_W corresponds to a balance between the second and the third (i.e., the linear vorticity balance between vortex stretching and planetary advection: $fw_z = \beta v$). According to Blumsack (1973), L_H and L_W are the ''Hydrostatic–Lineykin'' and the ''western'' scales, respectively, but we find the name ''western-diffusive'' scale for L_W to be more explicit. Note that the dividing criterion

$$\sqrt{\frac{3A_H}{K_L}}R = \left(\frac{2A_H}{\beta}\right)^{1/3} \tag{3.18}$$

is equivalent to $3^{1/2}L_H = 2^{1/3}L_M$. In the following we name each layer by the name of its scale. MU called the first regime ''viscous'' and the second one, ''diffusive.'' These authors emphasize that the western-diffusive layer, L_W, can be much larger than the other layers. They also noticed that the linear vorticity balance

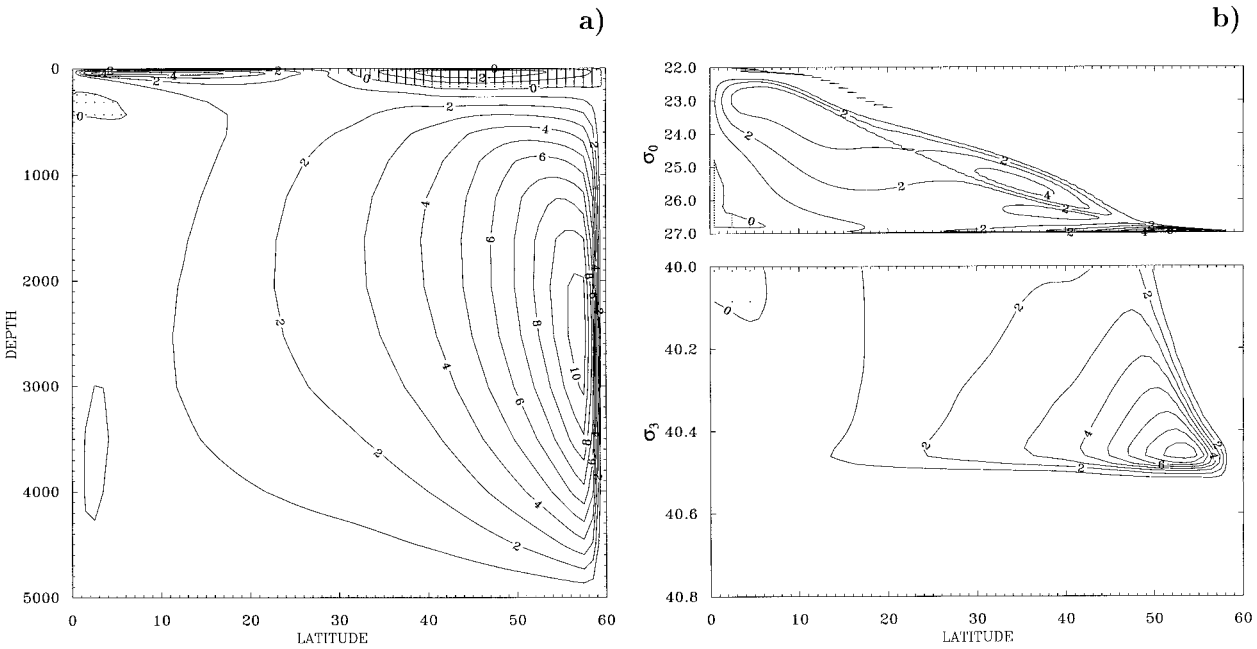

FIG. 2. Experiment HN. Depth coordinate meridional streamfunction (a). Density coordinate meridional streamfunction (b), where the zonal integration is performed along potential density surfaces referenced to the surface for low density range (upper panel) and referenced to 3000-m depth for high density range (lower panel). Dots and negative values indicate counterclockwise flow.

($fw_z = \beta v$) governing this layer implies that, in their 1½-layer model, upwelling is found for poleward western boundary current, while downwelling is found for equatorward flow. Therefore, they suggested that the interior downwelling below the thermocline observed in various model studies is related to an interior extension of the western boundary current governed by the diffusive regime with a large western scale. We now investigate their hypothesis with our OGCM.

4. Comparison of the numerical and analytical results

a. Laplacian diffusion representation of mesoscale eddy effect

We first look at simulations using the Laplacian formulation for mesoscale eddy effects. A manifestation of the Veronis effect is clearly dominating the meridional streamfunction in HN (Fig. 2a). Because a large part of the deep waters are brought back to the surface by the intense midlatitude WBL upwelling, less than three Sverdrups (Sv $\equiv 10^6$ m^3 s^{-1}) out of almost 11 Sv reach the southern half of the basin. This upwelling is balancing diffusive density fluxes, and therefore the computation of the streamfunction in density coordinates is relevant to illustrate its diapycnal nature. Following Hirst and McDougall (1998), we split the density coordinate streamfunction (Fig. 2b) into an upper part aimed at better describing the low density upper-ocean circulation (the potential density σ_0 is referenced to the surface) and a lower part appropriate to the high density range circulation (the potential density σ_3 is referenced to the 3000-m depth). The upper-ocean streamfunction is dominated by a large cell extending from the equator to 45°N that corresponds to the Ekman cell at low latitudes and to the subtropical gyre farther north. In this study we are concerned with the main overturning cell, which transports 9 Sv and confirms that most of the diapycnal upward movement happens north of 30°N. Recalling that the slope of the isolines gives a measure of the diapycnal nature of the flow, we will compare it in section 5b with experiment GMN. The vertical and horizontal velocity fields are shown for HN at 2700-m depth (Fig. 3). The patterns are representative of the circulation at intermediate depths, that is, between the bottom part of the main thermocline and the top of the abyss, from approximately 1500 to 3000 m. From 25° to 40°N, the western downwelling spreads progressively eastward while the western boundary layer upwelling (occupying a single grid point) strengthens by one order of magnitude to more than 10^{-5} m s^{-1}. As it appears in Holland's results and as noticed by MU, the interior downwelling at midlatitude closely corresponds to an equatorward flow (Fig. 3b). The continuity of the meridional equatorward flow from the western boundary to the interior corroborates the idea that the interior equatorward flow is part of the deep western boundary current (DWBC).

In order to test the validity of the theoretical explanation suggested by MU, the density as well as the vertical vorticity balances in the DWBC and the interior downwelling are compared with the analytical model

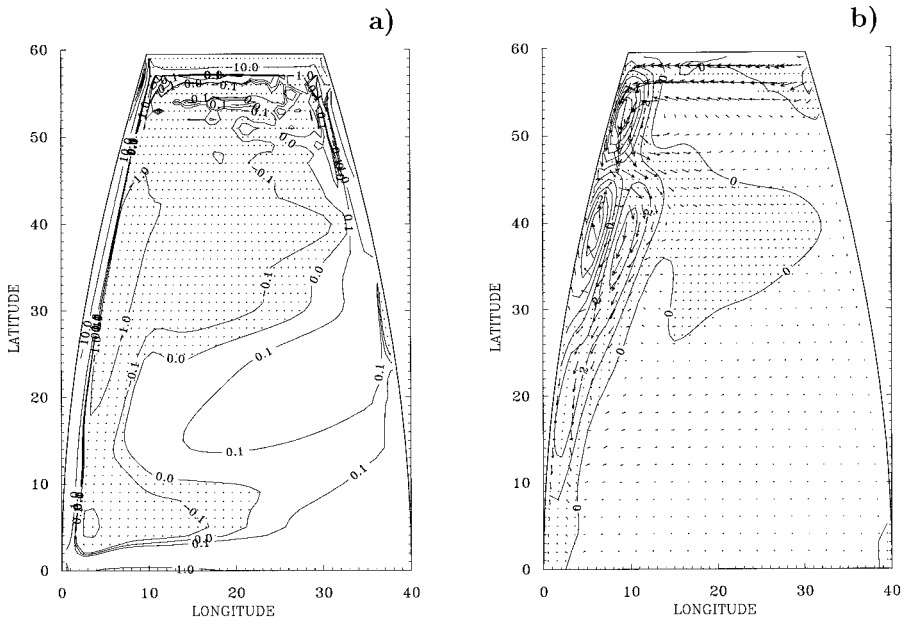

FIG. 3. Experiment HN. Vertical velocity at 2500-m depth (contour: 0.001, 0.1, 0, 1, 10 $x \pm 10^{-5}$ m s^{-1}), shaded areas correspond to downwelling (a). Meridional component of the velocity (in 10^{-3} m s^{-1}) superimposed on the horizontal velocity vector (max. vec.: 7×10^{-3} m s^{-1}) at 2700-m depth, shaded areas correspond to equatorward flow (b).

hypothesis. At mid and low latitudes at middepths, the main density balances are very close to the heat balance due to the strong similarities between temperature and salinity fields. It is therefore sufficient to examine the trends for the temperature equation. For a better description of the fine geographical diversity of the heat balances, three main regions have been distinguished (Fig. 4): region 1 (the western boundary layer), region 2 (the western region), and region 3 (the interior). Each of regions 1 and 2 is characterized by a specific dominant heat balance. In region 3 downwelling and upwelling may coexist and in this situation there are two different heat subregimes, one associated with downwelling and another with upwelling. In this paper, only the part of region 3 characterized by downwelling (called region 3^-) will be studied. In a given region, each trend is horizontally averaged and, for the sake of clarity, is normalized by the value of the largest trend at each model level. The horizontal advection trend includes both meridional and zonal terms but it is mainly representative of the meridional one, which dominates the western part of the basin. The vertical profiles for the three regions are shown along with their normalization factors in Fig. 5. Lateral mixing appears everywhere to be a dominant term. It is essentially compensated by the cold upwelling in region 1 (Fig. 5a), as found by Veronis (1975) through a scaling analysis. Hereafter, this heat balance will be referenced by the symbol K_L/W^+. In region 2, lateral mixing is balanced by warm downwelling (Fig. 5b). And in region 3^-, the interior downwelling region, the downward diffusive flux is significant but lateral cold mixing still necessitates an important vertical warm advection term (Fig. 5c). We call this the K_L/W^- heat regime. The dominance of the K_L/W^- heat regime over the interior downwelling region is confirmed by HC. In this experiment, region 3^- has the same extension but, due to the smaller K_V,

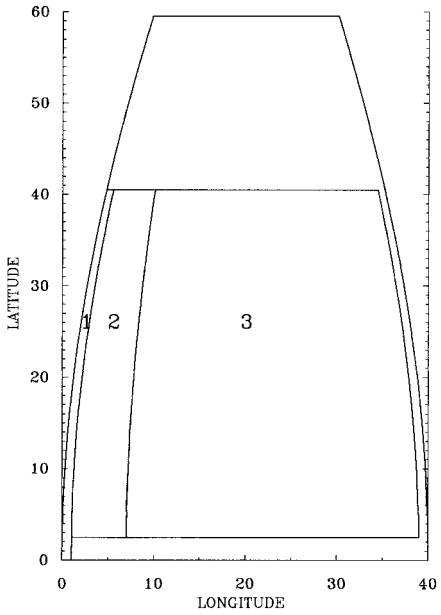

FIG. 4. Extension of the three regions analyzed in terms of heat balances; region 1, 2, and 3 are called the western boundary layer, western region, and interior, respectively.

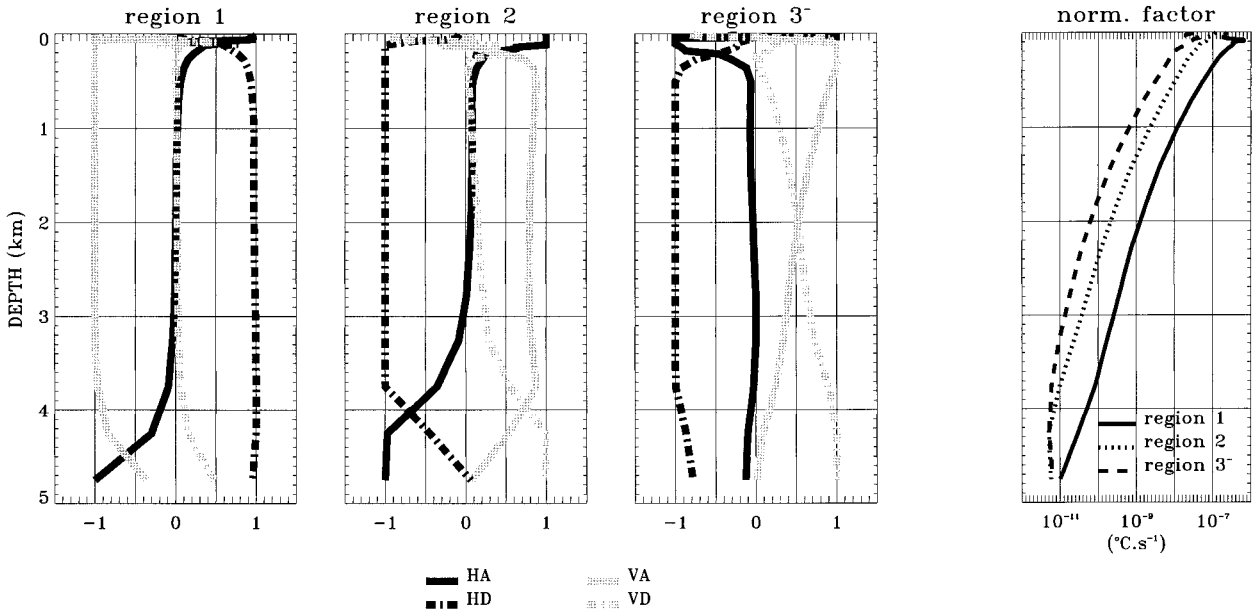

FIG. 5. Experiment HN. Normalized horizontally averaged temperature trends for regions 1 (a), 2 (b), and 3⁻ (c), and normalization factors (d) as a function of depth. HA and VA stand for horizontal and vertical advection, HD and VD for horizontal and vertical diffusion.

the downward diffusion is negligible (Fig. 6). In conclusion, as assumed in the analytical model [Eq. (3.5)] and as shown by Veronis for Holland's results (1971), in the middepth ranges the vertical advective and lateral diffusive terms dominate the western part of the basin, including the interior region characterized by negative vertical velocities. Note that both the upper ocean (above 500 m) and the abyss can present different heat balances than the middepths. The advection trend may especially become a major term, meaning that the analytical model rationalization is not straightforward there (a point already suggested by Warren 1976).

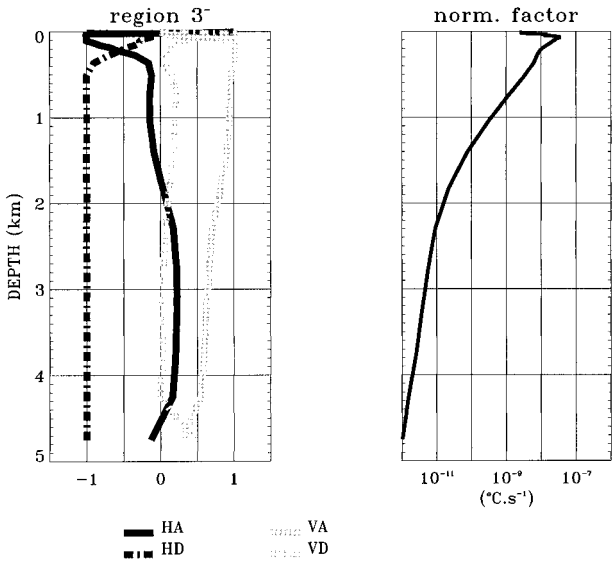

FIG. 6. Experiment HC. Normalized horizontally averaged temperature trends for the interior downwelling region 3⁻ (a) and normalization factor (b); otherwise as for Fig. 3.

The vertical vorticity regimes are now studied in order to check whether the three balances and the zonal scales of the DWBC given by the analytical model are observed. The three principal vertical vorticity trends $A_H\Delta\zeta$, $-\beta v$, and fw_z are presented at 2700 m (Fig. 7), the other terms being negligible. Below 20°N along the western wall, the vortex stretching term is weak and the dominant balance involves relative vorticity diffusion and planetary advection (region A). This equilibrium, $\beta v = A_H\Delta\zeta$, corresponds to the Carrier–Munk layer L_M and holds over the width of the DWBC. As stated by MU, the intensification of the interior northward flow along the DWBC at these latitudes and the shrinking to the north (near 30°N) of the interior southward flow are the recirculations typical of the sinusoidal Munk solution.

Around 20°N, the DWBC splits into two lateral layers. One is a very thin layer over the first grid point along the wall (region B). It is clearly dominated by the balance $A_H\Delta\zeta = -fw_z$ involving a negative diffusion term (the wall reduces the relative vorticity) and a positive vortex stretching (associated with the intense single gridpoint upwelling). The other layer is widening with latitude and coincides with the extension of the downwelling in the interior (region C). It is mainly governed by the $\beta v = fw_z$ equilibrium where planetary advection is positive (equatorward flow) and the vortex stretching is negative (associated with the negative vertical velocities). An exact equilibrium between two terms is never achieved, so all three trends are important, but one of them is always significantly smaller. This morphology is in good qualitative agreement with the analytical model results un-

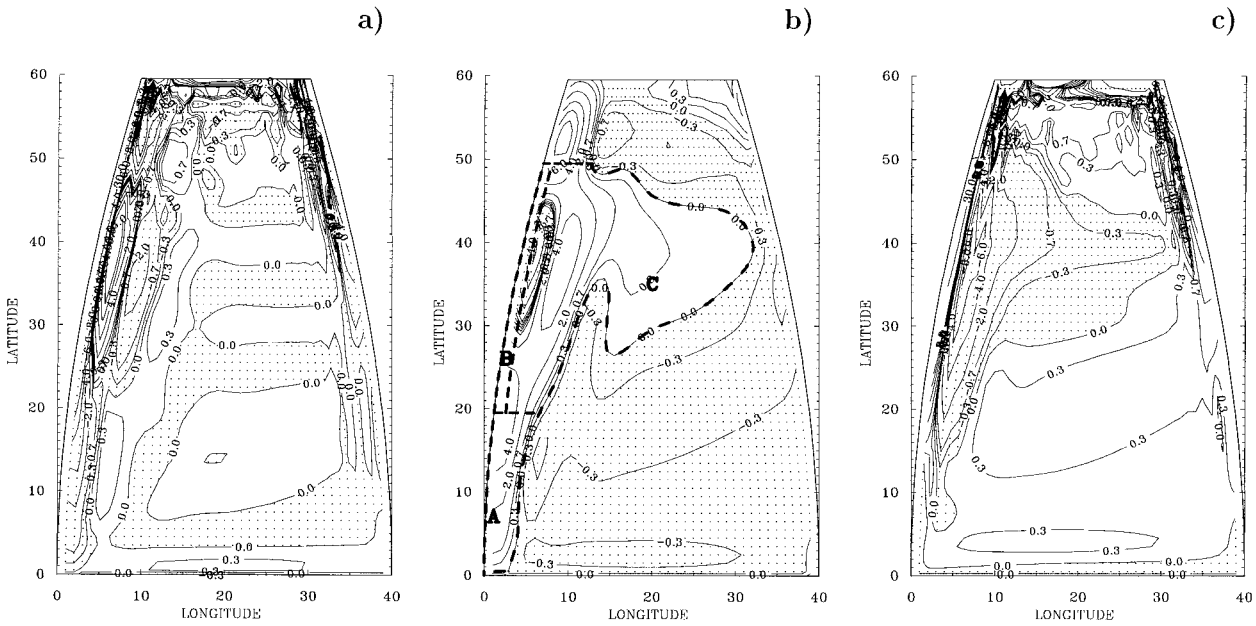

FIG. 7. Experiment HN. Vertical vorticity trends at 2700-m depth (in 10^{-14} s^{-2}), shaded areas correspond to negative values, horizontal dissipation $A_H\Delta\zeta$ (a), planetary advection $-\beta v$ (b), and vortex-stretching term fw_z (c). Regions A, B, and C are demarcated by dashed lines in (b) (see text for details).

derlined by MU: the DWBC baroclinic scale splits with latitude from a Carrier–Munk layer L_M into a Hydrostatic–Lineykin layer L_H and a western-diffusive layer L_W.

The agreement with theory is now examined from a quantitative point of view. Due to the exponential form of the analytical solutions, it is necessary to multiply the *e*-folding scales by a factor of 2 to 3 to evaluate a width for the horizontal current structures. The value of L_M ($=[A_H/\beta]^{1/3} \approx 120$ km) yields a width of ~300 km corresponding roughly to the extension of the DWBC below 20°N (Fig. 3b). At 40°N, the calculation for L_H ($=R[A_H/K_L]^{1/2} \approx 70$ km) yields a Hydrostatic–Lineykin layer supposedly extending over ~200 km. This value is not unrealistic in regard to the single gridpoint extension of the western boundary layer upwelling and considering the coarseness of the resolution (Fig. 3a). The expression of L_W ($=K_L/\beta R^2$) gives a rapidly widening scale with latitude because of the strong latitude dependence of the denominator: it enlarges from 40 km at 10°N to 400 km at 40°N and 870 km at 45°N. The last two values, multiplied by 3, compare favorably with the zonal extension of the DWBC at midlatitudes. Lastly, the criterion dividing the two regimes [$3^{1/2}L_H = 2^{1/3}L_M$, Eq. (3.18)] gives a characteristic latitude of about 30°N, while the splitting of the DWBC is observed around 20°N. As expected from previous studies, the reduction of K_L in HrN produces coherent results: the DWBC is zonally confined to the first 500–1000 km approximately, and the associated downwelling has an extension significantly reduced by a factor 2 to 3 (not shown). Note that, according to the expression for L_W, the reduction of the DWBC and the downwelling should reach a factor 4. Hence the comparison reveals that the analytical model can give satisfying order-of-magnitude results, considering its simplicity.

These numerical results show that the ubiquitous interior downwelling can be rationalized. For the sets of parameters used in our study, the shape, the scale, and the localization of this feature are given to first order by the analytical linear model used in the study done by MU and also under slightly different forms in previous works (e.g., Pedlosky 1969; Warren 1976; Edwards and Pedlosky 1995). This phenomenon, as reported in the literature, is strongly dependent on the horizontal mixing term representing mesoscale eddy effects. As shown by Gough and Lin (1995), the use of isopycnal mixing significantly mitigates the interior downwelling but this mitigation is limited by the background horizontal diffusion term they used for numerical stability. Because the GM formulation precisely eliminates the need for a background term (e.g., GM; Hirst and McDougall 1996), it is natural to wonder how it corrects the Veronis effect.

b. GM representation of mesoscale eddy effects

Böning et al. (1995; personal communication 1998) and Danabasoglu and McWilliams (1995) showed that when the GM parameterization is used, the depth-coordinate meridional streamfunction associated with the Eulerian-mean velocities does not display the anomalous intense western boundary layer upwelling associated with the Veronis effect. This is also the case in

GMN (Fig. 8a) accompanied by a drastic reduction of the overturning rate. Hence, such changes could be partly interpreted as a consequence of the disappearance of the Veronis effect and its upwelling/downwelling system when mesoscale eddy effects are no longer represented by diffusion. On the density coordinate streamfunction (Fig. 8b), strong modifications are also observed. The upper panel displays a significant negative cell in the northern half of the basin, which corresponds to the northern Ekman cell. It was mainly confined to the homogenous mixed layer in HN and therefore hardly visible in density coordinates, but the eddy-induced advection stratified the surface layers (see discussions of this effect in Hirst and Caï 1994; Hirst and McDougall 1996) and consequently expanded the density range covered by this cell. In the lower panel of Fig. 8b, the reduction of the main overturning cell and its midlatitude diapycnal upwelling is comparable to Fig. 8a but, interestingly, between 30° and 40°N, there is a small cell showing that there is still downward diapycnal movement in this latitude band. The density coordinate streamfunction seems to indicate that the Veronis effect is still at play in this experiment. An examination of the corresponding Eulerian-mean velocity field below the thermocline (Fig. 9) indicates that this is the density coordinate that gives the best insight: the location as well as the intensity of both the interior downwelling and the WBL upwelling are almost unchanged compared to HN (Fig. 3a). The same is true for the horizontal currents. Hence, the GM parameterization with a rather strong eddy diffusivity is associated with a velocity structure that is locally very similar to the one related to the Laplacian operator with the same diffusivity, especially the interior downwelling and WBL upwelling patterns.

This similarity can be understood by looking again at the temperature trends for GMN, including the eddy-induced horizontal and vertical advection terms (Fig. 10). At intermediate depths, both the induced horizontal advection and isopycnal diffusion appear to make small contributions. In fact, the thermal regimes are close to those of HN if one mentally substitutes the horizontal diffusion for the eddy-induced vertical advection (cf. Figs. 10 and 5). Hence it appears that the similarities between the circulations in HN and GMN are due to the domination of the GM parameterization by its vertical advection component, the latter producing an effect on the temperature field very close to the horizontal diffusion term. Since this parameterization depends on the same parameter K_L, the heat regimes of the WBL upwelling and the interior downwelling may be described by the same symbols K_L/W^+ and K_L/W^-. This similarity can be rationalized following the study by Treguier et al. (1997) if one considers two characteristics of the two simulations: the quasigeostrophy (QG) of the large-scale currents in the interior and the use of a common and uniform thickness diffusivity K_L. Indeed, developing the expression of the eddy-induced advection of density when K_L is constant gives

$$\mathbf{U}_h^* \cdot \nabla_h \rho = -K_L(\underbrace{\nabla_h \rho_z \cdot \mathbf{S}}_{\text{(i)}} - \underbrace{\rho_{zz}|\mathbf{S}|^2}_{\text{(ii)}}),$$

$$w^* \rho_z = -K_L(\underbrace{\Delta_h \rho}_{\text{(iii)}} + \underbrace{\nabla_h \rho_z \cdot \mathbf{S}}_{\text{(i)}}).$$

In the QG limit, terms (i) and (ii) are negligible and the trend of the eddy-induced advection of density reduces to horizontal diffusion in the interior ($-\mathbf{U}^* \cdot \nabla \rho = K_L \Delta_h \rho$). This identity implies that Eulerian-mean circulation patterns verifying the QG density hypothesis (i.e., horizontal variations of the density field are negligible compared with its vertical variations) will locally not be strongly modified by a switch from one closure to the other, assuming a common constant value for K_L. We numerically checked that terms (i) and (ii) are much smaller than (iii) in GMN, except at high latitudes where density varies strongly laterally and near the bottom and the surface where the isoneutral slope $|\mathbf{S}|$ are rapidly set to zero. Thus, the Eulerian-mean circulation at intermediate depths in GMN can be rationalized with the analytical model in the same way as before. The situation is different for GMrN where K_L is four times smaller below the thermocline and the lateral density gradients can be much stronger. It corresponds to a loss of quasigeostrophy and thus to weaker local similarities in the heat fluxes produced by the two parameterizations. Accordingly, the heat balances as well as the dynamics patterns are less similar to HrN, especially near the DWBC steep isopycnal slopes (not shown). Nevertheless, the strong similarities between HN and GMN are local and, as seen in the overturning streamfunctions, an important difference between the two experiments is that the WBL upwelling signal disappears after zonal averaging over the basin in GMN. An explanation of this is given in the next section.

5. Interpretation and discussion

The above rationalization of the upwelling/downwelling system provides the necessary elements to predict to first order the location and shape of this pattern in the experiments described above as a function of the stratification and mixing parameters. In this section, we develop an interpretation of the phenomenon aimed at better understanding the physics.

a. Laplacian diffusion case

First consider the situation when Laplacian diffusion is used. We showed that in the interior downwelling region, the downward diffusive heat flux is unable to equilibrate the cold trend maintained by horizontal mixing with the DWBC cold waters (Fig. 5). It is the downward advection of warm upper waters that closes the heat balance. We therefore conclude that the interior

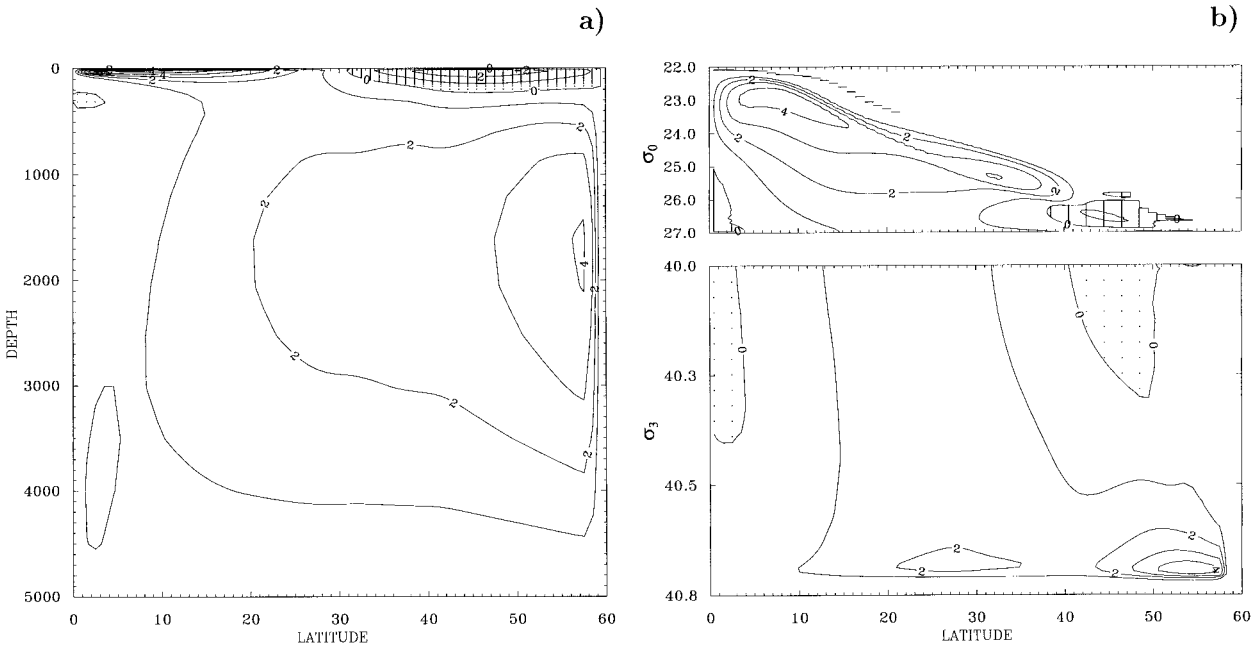

FIG. 8. Eulerian-mean meridional streamfunctions for GMN; otherwise as for Fig. 2.

downwelling forms the complement, in terms of heat balance, of the WBL upwelling. The horizontal diffusion across the slopes of the DWBC warms the WBL and requires an upward cooling movement across the stratification, while it cools the interior and requires a corresponding downward advection. Hence, while Veronis showed that the mechanism at work for the WBL upwelling is what we called K_L/W^+, our study points out the existence of an antisymmetrical K_L/W^- heat flux mechanism at work for the interior downwelling. The dominance of these two opposite forms of the lateral diffusion/vertical advection heat balance agrees well with the analytical model rationale, one of the keystones of which is precisely the K_L/W density equilibrium.

Such a heat fluxes reasoning helps to understand some major characteristics of the phenomenon that were unexplained with the mass continuity argument of Veronis. Consider first its geographical location. Due to the mainly meridional orientation of the DWBC, the downwelling must be located in the same latitude band as the

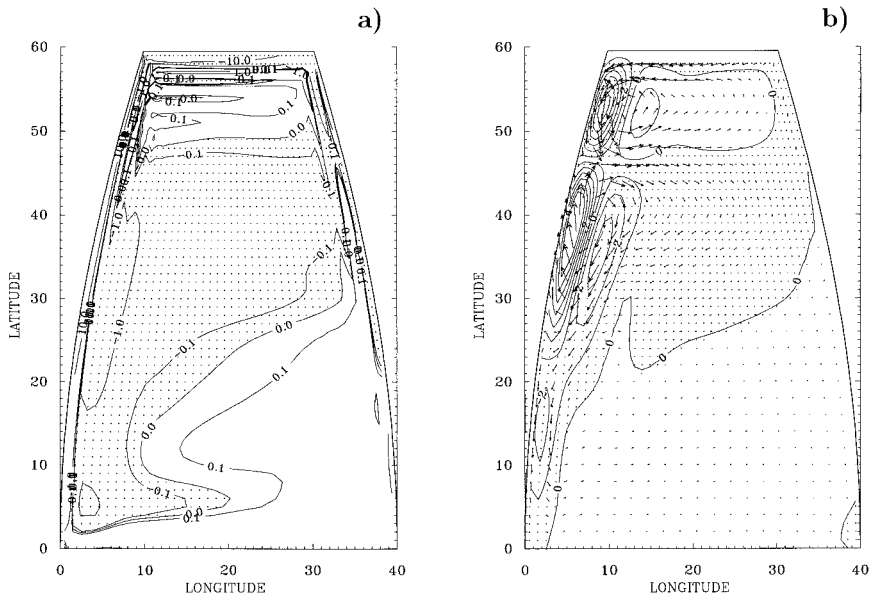

FIG. 9. As for Fig. 3 but for the Eulerian-mean circulation in GMN.

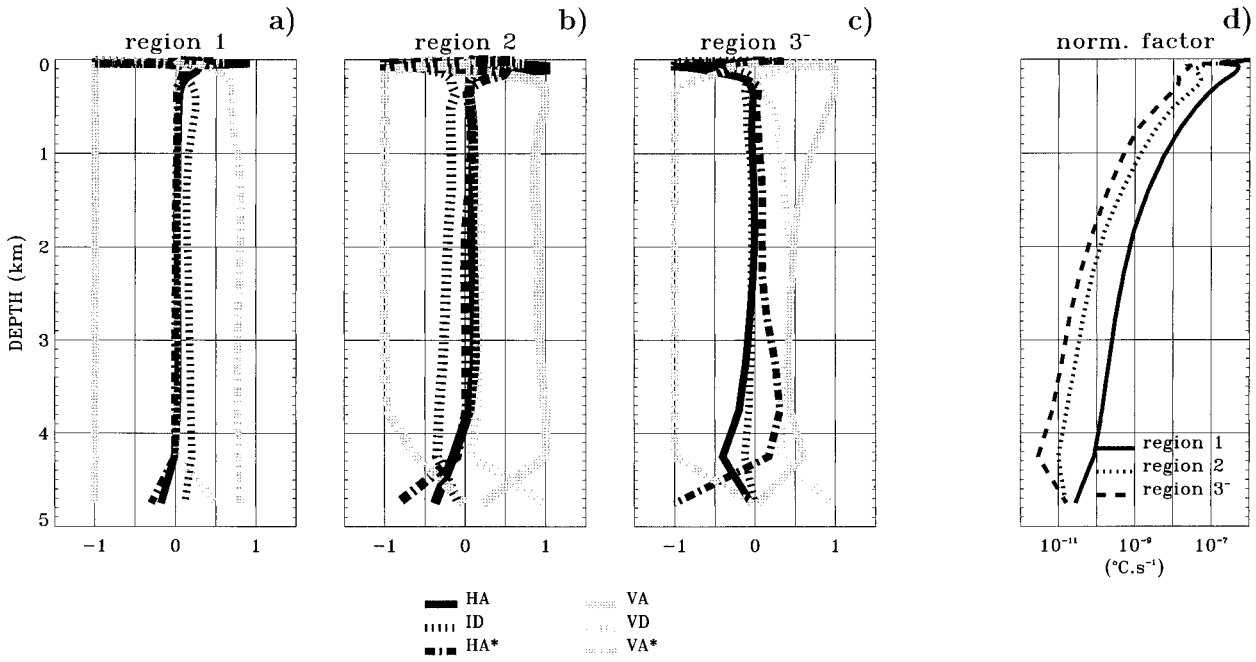

FIG. 10. Experiment GMN. Normalized horizontally averaged temperature trends in function of depth for regions 1 (a), 2 (b), and 3^- (c), and normalization factors (d) as a function of depth. HA and VA stand for horizontal and vertical advection, ID and VD for isopycnal and vertical diffusion, and HA* and VA* for eddy-induced horizontal and vertical advection.

WBL upwelling and next to it, on the other side of the DWBC core. Then consider the weakness of the downwelling intensity and its large zonal extension compared to the upwelling. While the presence of the wall generates a strong convergence of the westward positive heat flux at the boundary and therefore requires an intense cold advection there, the eastern boundary is far away. Hence, the eastward negative heat flux experiences a much weaker convergence and acts over a larger distance. Consequently the balancing vertical advection is less intense and must occur over a correspondingly larger distance. The K_L/W^- mechanism, its antisymmetrical companion K_L/W^+, and the physics invoked here are illustrated in Fig. 11a.

b. GM parameterization case

Consider now the analogous phenomenon observed in the Eulerian-mean circulation in GMN. As shown by Gent et al. (1995), the GM parameterization acts to flatten density fronts by advecting cold water toward where it is warm and vice versa. As demonstrated earlier, this effect is essentially dominated by vertical advection on both sides of the DWBC core. Hence, downward-induced advection near the wall tends to lower isopycnals, while upward induced advection tends to raise them offshore. For the circulation to stay in a stationary equilibrium, the Eulerian-mean currents have to counteract this vertical movement by forming an opposite WBL upwelling and interior downwelling system (Fig. 11b). The amplitude and extension of this response is then driven by that of the induced transport system, itself controlled by the value of the thickness diffusivity. This explanation is supported by the eddy-induced vertical velocity field at 2500-m depth in Fig. 12a. South of 40°N, the intensities of the eddy-induced field compare well and are opposite in sign to the Eulerian-mean field in the region of the WBL upwelling/interior downwelling system. A comparable situation of opposite patterns between Eulerian-mean and eddy-induced circulation were observed by Danabasoglu and McWilliams (1995) for the Southern Ocean meridional Deacon cell. Similar to the DWBC, the Circumpolar Current is associated with strongly sloping isopycnals, and accordingly horizontal diffusion is a major cause of the Deacon cell (Hirst et al. 1996) in coarse-resolution models. It is therefore very probable that the density front flattening mechanism described above is at work in World Ocean low-resolution models.

At this point, it is important to recall that this is the so-called effective transport, the sum of the Eulerian-mean and induced transport, which affects the tracers in the model. Following our notation, the two former antisymmetrical mechanisms K_L/W^+ and K_L/W^- at work in HN become in GMN, respectively W^-/W^+ and W^+/W^- (or more precisely W^{*-}/W^+ and W^{*+}/W^-). The effective vertical transport associated with them can be described in turn by the symbolic identities $W^+/W^- = W^-/W^+ \approx 0$. In other words, the Eulerian-mean and eddy-induced transports should cancel each other and therefore favor an effective circulation less controlled by the parameterization of mesoscale eddy effects, clos-

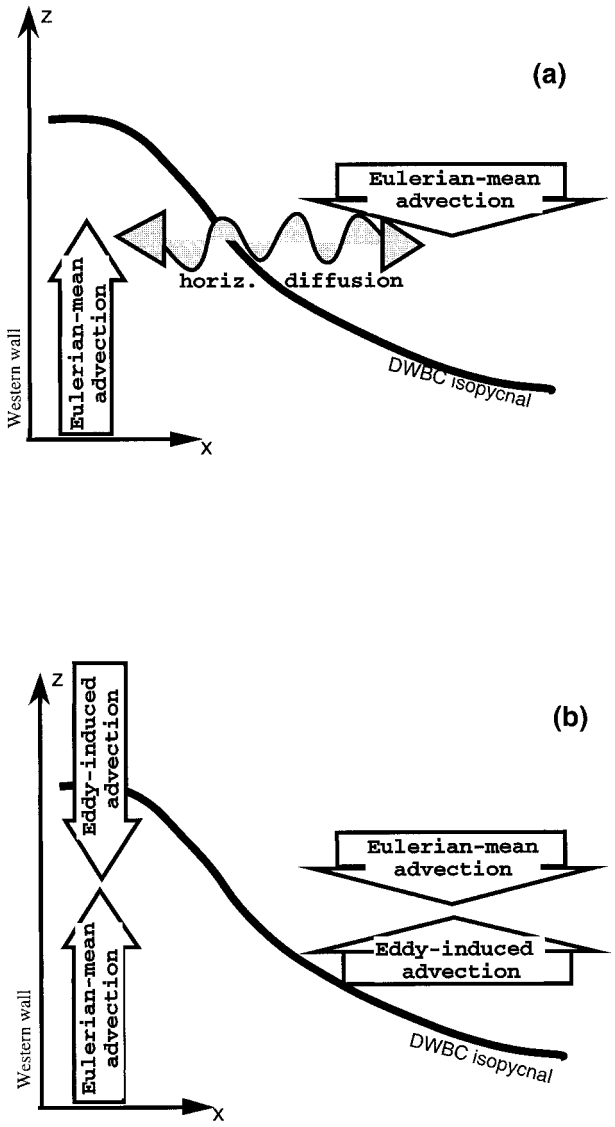

FIG. 11. Illustration of the heat balance mechanisms at work for the WBL upwelling/interior downwelling system when the Laplacian formulation is used (a) and when the eddy-induced velocity formulation is used (b). Arrows symbolize heat fluxes.

er to the SA one. Figure 12b shows the corresponding effective vertical velocity field. As expected, south of 40°N, the field is free of the strong WBL upwelling/interior downwelling system. A similar nullification phenomenon occurs for the Deacon cell in Danabasoglu and McWilliams (1995) study and is also reported by Robitaille and Weaver (1995). As a result in our experiment, the effective circulation in the western part of the basin is characterized by a much less intense WBL upwelling than before (one order of magnitude weaker than in HN), governed by a heat balance between isopycnal mixing and effective vertical advection, and an interior upwelling governed by a more traditional heat balance between diffusion and effective advection on the vertical (not shown).

Interestingly, despite the resemblance of the interior effective vertical movement and heat balance with the SA reconstruction of the deep circulation, the effective horizontal flow displays some original patterns (Fig. 12c). Between 20° and 40°N, the interior does not have a significant poleward flow as expected from the linear vorticity balance ($fw_z = \beta v$), but rather a fully westward one. This discrepancy can be understood if one notices that the induced velocities are not geostrophic by construction. Hence they confer an ageostrophic character to the currents, which in coarse-resolution models are geostrophic at a very good approximation except along the boundaries and close to the equator (Lazar 1997). The significance of the ageostrophic component depends upon the value of the thickness diffusivity K_L. Here, this midlatitude westward flow is weakly controlled by stretching due to the interior upwelling and mainly by the ageostrophic induced velocity tending to flatten out the zonal slope related to the interior extension of the Eulerian-mean DWBC.

We now explain why the WBL upwelling signal is strongly weakened in the Eulerian-mean meridional streamfunction in GMN, as was the case in Böning et al. (1995, their Fig. 1b). The GM vertical velocities are the derivatives of the potential $K_L\mathbf{S}$, which is related to the slope of the neutral surfaces (see §2b). Because the slopes along the western wall are essentially zonal, this is mainly the zonal derivative of the zonal component of the potential ($K_L\partial_x S_x$), which produces the induced WBL downwelling/interior upwelling system. Therefore, when integrated over the basin width, this induced system reduces simply to a term proportional to the difference between the two values of S_x at the meridional boundaries

$$K_L\left(S_x|_{\substack{\text{eastern}\\\text{boundary}}} - S_x|_{\substack{\text{western}\\\text{boundary}}}\right).$$

The potential being set to zero at the walls (no net flow through solid boundaries), the system vanishes, which corresponds, of course, to a cancellation of the induced upwelling by its companion downwelling. Following our argument, the responding (opposite) Eulerian-mean current system will vanish in a comparable manner. Consequently, the main part of the WBL upwelling will be canceled by the interior downwelling in the Eulerian-mean meridional streamfunction. Note that in this case the argument of Veronis applies precisely in the sense that the interior downwelling is effectively mass-balancing the WBL upwelling. As suggested by one reviewer, the reduction of the meridional transport could also be partly due, via the thermal wind equation, to the tendency of the eddy-induced transport to flatten isopycnals and reduce horizontal (in this case zonal) density gradients. The strong stability of the intensity of the southward DWBC at middepth between HN and GMN (cf. Figs. 3b and 9b) indicates that this effect is

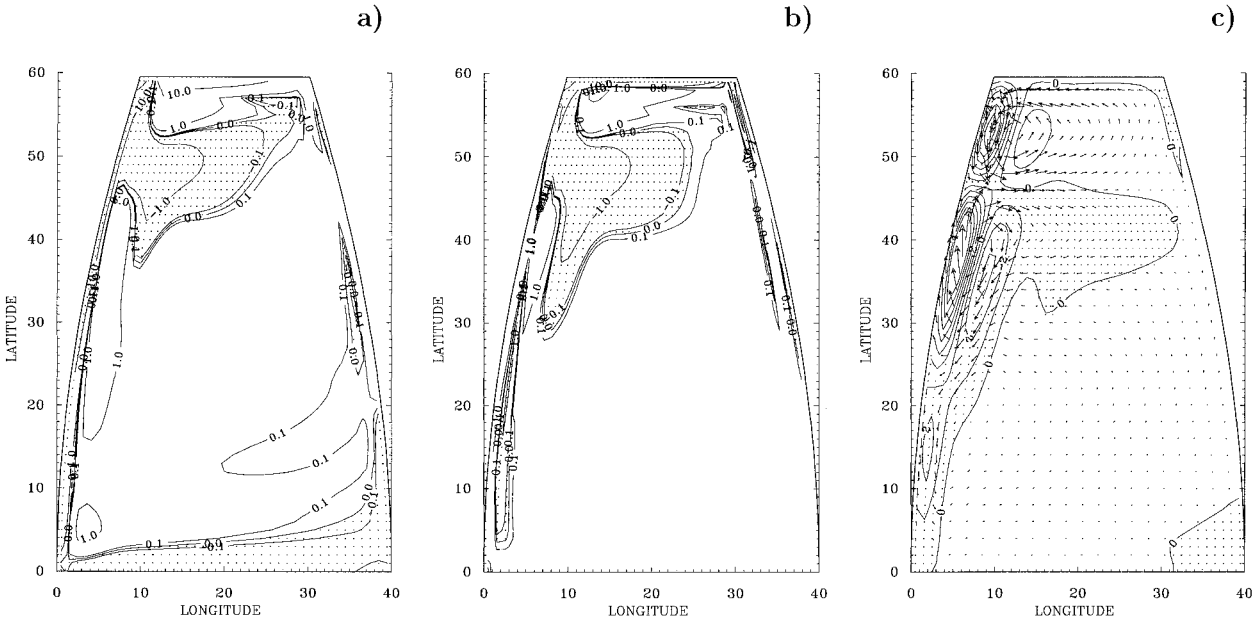

FIG. 12. Experiment GMN. Vertical velocities, induced (a) and effective (b) at 2500-m depth [contour: 0.1, 0, 1, 10 ($x \pm 10^{-5}$ m s^{-1}], shaded areas corresponds to downwelling. (c) Meridional component of the effective velocity (in 10^{-3} m s^{-1}) superimposed on the horizontal effective velocity vector (max vector: 7×10^{-3} m s^{-1}) at 2700-m depth, shaded areas correspond to equatorward flow.

far from being dominant. Actually, the Eulerian-mean flow there counteracts the flattening tendency so that zonal density gradients are comparable in the two runs.

At this point, we can state that for flows closely approximating the quasigeostrophic density gradient hypothesis, the GM closure produces an upwelling/downwelling system comparable to the one associated with the Veronis effect. Meanwhile, by construction of the eddy-induced velocities, first the phenomenon's structure is modified in such a way that most of the Eulerian-mean response vanishes after zonal integration in the meridional streamfunction and, second, the eddy-induced heat fluxes are advective and thus can be canceled locally by the Eulerian-mean field. Therefore, the circulation experienced by tracers departs strongly from the one obtained with the traditional Laplacian approach. This is remarkably illustrated by the effective circulation streamfunctions in GMN. The depth coordinate overturning (Fig. 13a) displays only 4–5 Sv sinking at high latitudes and rising to the surface on the whole latitude range from 40°N to the equator. The comparison with Fig. 2a reveals, therefore, that 5 Sv circulating in the last northern 15° in HN were associated with the Laplacian formulation. The density-coordinate streamfunction leads to similar conclusions (lower panel in Fig. 13b). In addition, the comparison of the isoline slopes with those of HN (Fig. 2b) enlightens the much less diapycnal nature of the deep circulation: closer to the SA theory, the ascent of the deep waters toward the surface occurs more slowly and accordingly over a larger latitudinal extension.

The drop of about 50% in the upwelling and the overturning rate as well as the relative increase of the meridional mass exchange with low latitudes are also observed in the idealized basin of Weaver and Eby (1997). Comparable modifications occur in the Atlantic model used by Böning et al. (1995; personal communication, 1998) except that there is no change in the overturning rate. In the global ocean model of Danabasoglu and McWilliams (1995) the changes are similar to ours, but their amplitude is only about 15%. The discrepancy in the results compared with more realistic ocean models is perhaps to be found in the absence of Southern Hemisphere driving mechanisms for the overturning of single hemisphere basin models. The consequences on tracer distribution of local cancellation between Eulerian-mean and eddy-induced transport are manifest for chlorofluorocarbons (CFCs) in the Southern Hemisphere where the cancellation of the Deacon cell greatly reduces the CFC uptake and consequently improves their distribution (Robitaille and Weaver 1995; England 1995).

It is worthwhile to discuss some additional features of the effective circulation meridional streamfunctions related to eddy-induced velocities. First, the overturning rate and the upwelling in the depth coordinate representation are stronger than for the Eulerian mean (compare with Fig. 8). As noted by one reviewer, one could expect instead a reduction of the midlatitude upwelling, considering the cancellation mechanism between Eulerian-mean and eddy-induced velocities emphasized in this paper. We therefore recall that the cancellation of the upwelling/downwelling system happens in the plane orthogonal to the steep slope of the DWBC (here the

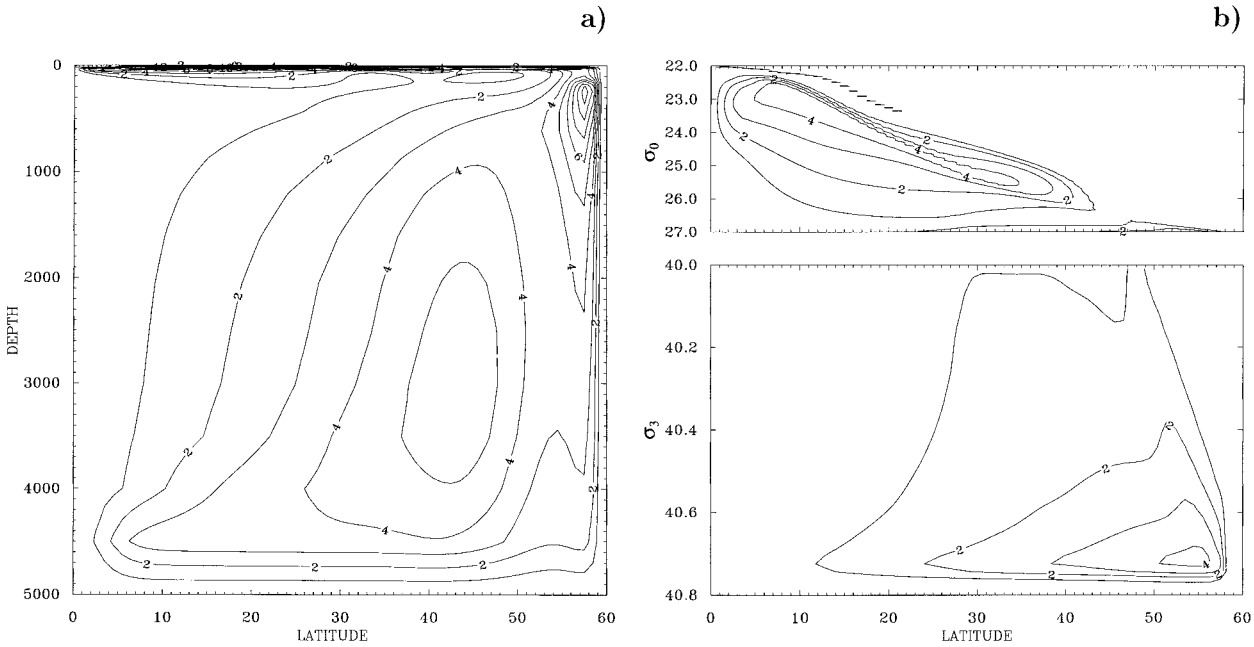

FIG. 13. Experiment GMN. Meridional streamfunctions of the effective circulation (Eulerian mean+eddy-induced velocity), otherwise as for Fig. 2.

x–*z* plane, as illustrated Fig. 11b). The intensification observed is confined to the *y*–*z* plane. It is due to eddy-induced velocities associated purely with the meridional positive slopes of the middepth isopycnal surfaces north of 25°–30°N, and it is not related to the Veronis effect (as explained above, eddy-induced velocities driven by zonal slopes cancel after zonal integration anyway). Böning et al. (1995; personal communication 1998) found that including eddy-induced velocities has only minor effects on the maximum overturning rate or the latitudinal structure (at the 1000-m level) of the meridional streamfunction. We believe that these authors did not find the increase mentioned above because of their weaker thickness diffusivity. A second point to discuss in the depth-coordinate streamfunction is the presence of two intense secondary cells located at the surface and along the northern boundary as well as a thin 3 Sverdrup flow along the bottom. These eddy-induced transport features result entirely from the imposed cancellation of the potential $K_L\mathbf{S}$ at the boundaries: the transition for slopes of neutral surfaces from the interior to the boundary null value occurs over a few grid points and corresponds therefore to strong eddy-induced velocities. This is a well-known problem of the GM parameterization near the surface (see section 2b), but it has not been described for the northern and bottom boundaries. A smaller K_L attenuates the intensity of the potential ($K_L\mathbf{S}$) shear in these regions, and these characteristics are accordingly significantly lessened in GMrN (not shown).

6. Conclusions

This study addresses the physics of the anomalous interior downwelling and the companion WBL upwelling, observed in several coarse-resolution ocean models at midlatitudes below the thermocline. These features are related to intense diapycnal diffusion of heat through horizontal mixing across the slope of the DWBC, as described by Veronis (1975). They are associated with significant errors in quantities important for climate modeling. We used an idealized OGCM and analytical arguments to demonstrate the validity, for our set of experiments in the middepth interval (1000–3000 m), of the analytical rationale proposed by MU in terms of baroclinic zonal length scale of the DWBC. Our analysis in terms of heat and vorticity balances suggests that it is possible, for the sets of parameters we used, to estimate rather accurately the occurrence of the interior downwelling, as well as its shape and extension as a function of the mixing coefficients. These results emphasize the complex and poorly known baroclinic dynamics of the DWBC and its morphology determined by three length scales, including the classical (but baroclinic) Munk (or Carrier–Munk) scale. A reasoning based on local heat balances shows that, in accord with the fundamental density balance of the analytical model, the interior downwelling is controlled by the balance K_L/W^- (lateral diffusion/downward advection), which is the antisymmetrical companion of the balance K_L/W^+ found by Veronis (1975) to be at work for the WBL upwelling. In contrast with the mass continuity reasoning used by Veronis, our heat balance argument allows

us to explain why the downwelling occurs next to the DWBC and why it is spreading into the interior.

As noted in previous studies, the use of the GM parameterization reduces the intensity of the signal of the WBL upwelling in the Eulerian-mean overturning streamfunction dramatically. Meanwhile, a local examination underlines some profound similarities between the local effects of the lateral mixing term and the GM parameterization terms on the Eulerian-mean circulation. It is shown that the quasigeostrophic character of the flow in the region of interest accounts for this result. Nevertheless, an essential breakthrough of the new parameterization is its advective character. It allows a major cancellation of the Eulerian-mean vertical advection by the eddy-induced advection (dominated by its vertical component) and yields a strongly modified effective circulation, and this is the effective circulation that tracers feel. Such a cancellation effect observed in the Southern Ocean Deacon cell (Danabasoglu and McWilliams 1995) has been found to greatly ameliorate the distribution of CFCs in the World Ocean (Robitaille and Weaver 1995; England 1995). At last we pointed out that, since the eddy-induced advection is not geostrophic, it introduces an ageostrophic component in the simulated currents.

We showed that the local similarity between heat fluxes produced by the eddy-induced velocities and the lateral diffusion operator (for the same diffusivity) are dependent on the quasigeostrophy of the temperature/density field. Therefore, the smaller the horizontal temperature/density gradients (compared to the vertical ones), the less the Eulerian-mean circulations will differ locally for two runs using the two parameterizations. As shown by Treguier et al. (1997) the quasigeostrophy of the flow is the limit when Laplacian diffusion and GM parameterization equal locally their effects on the temperature field away from the boundaries. In HrN and GMrN, the lateral diffusivity is small below the thermocline and thus allows significantly stronger lateral temperature/density gradients. This loss of quasigeostrophy corresponds accordingly to weaker local similarities in the heat fluxes produced by the two parameterizations and to different heat balances and circulation patterns. Generally speaking, between runs using one or the other formulation, one must expect to find the largest local discrepancies for the Eulerian-mean circulations at highest latitudes because the flow is less stratified (and also near the bottom and surface boundaries where eddy-induced velocities may become very strong). In addition, one must recall that net (or effective) fluxes undergone by tracers are *always* strongly different between runs using one or the other parameterization, regardless of the nature of the stratification. For the water mass properties, the switch from lateral mixing to eddy-induced advection confines their modification to a weak isopycnal mixing instead of a much stronger horizontal mixing and therefore significantly favors their conservation.

Regarding the rationalization of the DWBC dynamics, this study suggests that it is possible, using the dividing criterion (3.18) and the length scale expressions [(3.12), (3.15), and (3.16)] of the analytical model, to choose the lateral mixing coefficients for a simulation in order to obtain either the viscous vorticity regime or the diffusive one, determine the characteristic width of the DWBCs, and consequently set the proportion of the interior ocean dominated by downwelling and upwelling. This approach can also help to rationalize the sensitivity study performed by Böning et al. (1995) and Gough and Lin (1995) on the Veronis effect. In addition, this rationalization underlines the necessity for coarse ocean models used in climate studies to move beyond the traditional barotropic Munk scale and, instead, consider the dividing criterion and the three aforementioned baroclinic scales for setting the minimal horizontal grid size and horizontal viscosity coefficient of a simulation. This point was already raised by Colin de Verdière (1993). Indeed, depending on the mixing coefficients, the baroclinic western lateral deep boundary layer may become, for example, a Hydrostatic–Lineykin layer, which can be much smaller than the Carrier–Munk layer (in HN, the former is actually half the latter at 40°N). Our study also implies that analytical ocean models including a deep basin have to include the vortex stretching term in the vorticity equation in order to accurately simulate the dynamics of the deep western boundary.

Finally, it is important to say that, even if we now have a satisfying rationalization of the Veronis effect and its upwelling/downwelling system, the occurrence of these circulation patterns, a strong departure from the Stommel and Arons reconstruction, remains a strikingly open question for the real deep ocean. While the upwelling/downwelling system is often presented as an undesired artifact of eddy parameterizations, Warren (1981) recalls that it can, in fact, correspond to several features in the form of the deep currents, especially in the South Pacific (Warren 1976). Eddy-resolving simulations could provide some information concerning the persistence of such patterns with less influence from the parameterizations.

Acknowledgments. The authors would like to gratefully thank Profs. A. Colin de Verdière and O. Thual for helpful discussions and for their support during this study. Thanks also to Drs. Kevin Speer, Remy Tailleux, and David Walsh for fruitful comments. We gratefully acknowledge the programming support of Maurice Imbard during various stages of this work. We also thank two anonymous reviewers for their helpful comments. The computations were carried out on the CRAY94 and CRAY98 of IDRIS (Institut du Développement et des Ressources en Informatique Scientifique), Faculté des Sciences d'Orsay.

REFERENCES

Blanke, B., and P. Delecluse, 1993: Variability of the tropical Atlantic simulated by a general circulation model with two different mixed-layer physics. *J. Phys. Oceanogr.,* **23,** 1363–1388.

Blumsack, S. L., 1973: Length scales in a rotating stratified fluid on the beta plane. *J. Phys. Oceanogr.,* **3,** 133–138.

Böning, C. W., W. R. Holland, F. O. Bryan, G. Danabasoglu, and J. C. McWilliams, 1995: An overlooked problem in model simulations of the thermohaline circulation and heat transport in the Atlantic Ocean. *J. Climate,* **8,** 515–523.

Bryan, F. O., 1987: Parameter sensitivity of primitive equation ocean general circulation models. *J. Phys. Oceanogr.,* **17,** 970–985.

Bryan, K., 1984: Accelerating the convergence to equilibrium of ocean–climate models. *J. Phys. Oceanorgr.,* **14,** 666–673.

——, and A. H. Oort, 1984: Seasonal variability of the global water balance based on aerological data. *J. Geophys. Res.,* **89** (11), 717–730.

Colin de Verdière, A., 1993: On the oceanic thermohaline circulation. *Modelling Oceanic Climate Interactions,* J. Willebrand and D. L. T. Anderson, Eds., Springer-Verlag, 151–183.

Cox, M. D., 1987: Isopycnal diffusion in a z-coordinate model. *Ocean Model.,* **74,** 1–5.

Cummins, P. F., G. Holloway, and A. E. Gargett, 1990: Sensitivity of the GFDL ocean general circulation model to a parameterization of vertical diffusion. *J. Phys. Oceanogr.,* **20,** 817–830.

Danabasoglu, G., and J. C. McWilliams, 1995: Sensitivity of the global ocean circulation to parameterizations of mesoscale tracer transports. *J. Climate,* **8,** 2967–2987.

Edwards, C. A., and J. Pedlosky, 1995: The influence of distributed sources and upwelling on the baroclinic structure of the abyssal circulation. *J. Phys. Oceanogr.,* **25,** 2259–2284.

England, M. H., 1995: Using chlorofluorocarbons to assess ocean climate models. *Geophys. Res. Let.,* **22,** 3051–3054.

Esbensen, S. K., and V. Kushnir, 1981: *The Heat Budget of the Global Ocean: An Atlas Based on Estimates from Marine Surface Observations.* Rep. 29, Climatic Research Institution, Oregon State University, 27 pp.

Gargett, A. E., 1984: Vertical eddy diffusivity in the ocean interior. *J. Mar. Res.,* **42,** 359–393.

Gent, P. R., and J. C. McWilliams, 1990: Isopycnal mixing in ocean circulation models. *J. Phys. Oceanogr.,* **20,** 150–155.

——, J. Willebrand, T. J. McDougall, and J. C. McWilliams, 1995: Parameterizing eddy-induced tracer transports in ocean circulation models. *J. Phys. Oceanogr.,* **25,** 463–474.

Gerdes, R., C. Koberle, and J. Willebrand, 1991: The influence of numerical advection schemes on the results of ocean general circulation models. *Climate Dyn.,* **5,** 211–226.

Gill, A. E., 1973: Circulation and bottom-water production in the Weddell Sea. *Deep-Sea Res.,* **20,** 111–140.

Gough, W., 1997: Isopycnal mixing and convective adjustment in an ocean general circulation model. *Atmos.-Ocean,* **35,** 495–511.

——, and W. Welch, 1994: Parameter space exploration of an ocean general circulation model using an isopycnal mixing parameterization. *J. Mar. Res.,* **52,** 773–796.

——, and C. Lin, 1995: Isopycnal mixing and the Veronis effect in an ocean general circulation model. *J. Mar. Res.,* **53,** 189–199.

Hellerman, S., and M. Rosenstein, 1983: Normal monthly wind stress over the world ocean with error estimates. *J. Phys. Oceanogr.,* **13,** 1093–1104.

Hirst, A. C., and W. Cai, 1994: Sensitivity of a World Ocean GCM to changes in subsurface mixing parameterization. *J. Phys. Oceanogr.,* **24,** 1256–1279.

——, and T. J. McDougall, 1996: Deep-water properties and surface buoyancy flux as simulated by a z-coordinate model including eddy-induced advection. *J. Phys. Oceanogr.,* **26,** 1320–1343.

——, and ——, 1998: Meridional overturning and dianeutral transport in a z-coordinate ocean model including eddy-induced advection. *J. Phys. Oceanogr.,* **28,** 1205–1223.

——, D. R. Jackett, and T. J. McDougall, 1996: The meridional overturning cells of a World Ocean model in neutral density coordinates. *J. Phys. Oceanogr.,* **26,** 775–791.

Holland, W. R., 1971: Ocean tracer distributions. Part I. A preliminary numerical experiment. *Tellus,* **23,** 371–391.

Jackett, D. R., and T. J. McDougall, 1995: Minimal adjustment of hydrographic data to achieve static stability. *J. Atmos. Oceanic Technol.,* **12,** 381–389.

Lazar, A., 1997: La branche froide de la circulation thermohaline: Sensibilité à la diffusion dans un modèle de circulation générale idéalisée. Thèse de l'Université Paris 6, 269 pp.

Ledwell, J. R., A. J. Watson, and C. B. Law, 1998: Mixing of a tracer in the pycnocline. *J. Geophys. Res.,* **103,** 21 499–21 529.

Levitus, S., 1982: *Climatological Atlas of the World Ocean.* NOAA Prof. Paper No. 13, U.S. Dep. of Commerce, NOAA 173 pp.

Madec, G., and M. Imbard, 1996: A global ocean mesh to overcome the North Pole singularity. *Climate Dyn.,* **12,** 381–388.

Masuda, A., and K. Uehara, 1992: A reduced-gravity model of the abyssal circulation with Newtonian cooling and horizontal diffusion. *Deep-Sea Res.,* **39,** 1453–1479.

McWilliams, J. C., and P. R. Gent, 1994: The wind-driven ocean circulation with an isopycnal-thickness mixing parameterization. *J. Phys. Oceanogr.,* **24,** 46–65.

Munk, W. H., 1950: On the wind-driven ocean circulation. *J. Meteor.,* **7,** 79–93.

——, 1966: Abyssal recipes. *Deep-Sea Res.,* **13,** 707–730.

Olbers, D. J., M. Wenzel, and J. Willebrand, 1985: The inference of North Atlantic circulation patterns from climatological hydrographic data. *Rev. Geophys.,* **23,** 313–356.

Pedlosky, J., 1969: Linear theory of the circulation of a stratified ocean. *J. Fluid Mech.,* **1,** 185–205.

Redi, M. H., 1982: Oceanic isopycnal mixing by coordinate rotation. *J. Phys. Oceanogr.,* **12,** 1154–1158

Robitaille, D. Y., and A. Weaver, 1995: Validation of sub-grid-scale mixing scheme using CFCs in a global ocean model. *Geophys. Res. Lett.,* **22,** 2917–2920.

Stommel, J., and A. B. Arons, 1960b: On the abyssal circulation of the World Ocean-II. An idealized model of the circulation pattern and amplitude in oceanic basins. *Deep-Sea Res.,* **6,** 217–233.

Suginohara, N., and S. Aoki, 1991: Buoyancy-driven circulation as horizontal convection on β plane. *J. Mar. Res.,* **49,** 295–320.

Toggweiler, J. R., K. Dixon, and K. Bryan, 1989: Simulations of radiocarbon in a coarse-resolution world ocean model 2. Distribution of bomb-produced carbon-14. *J. Geophys. Res.,* **94,** 8217–8242.

Toole, J. M., 1998: Turbulent mixing in the ocean. *Ocean Modeling and Parameterization,* E. P. Chassignet and J. Verron, Eds., NATO Science Series C, Kluwer Academic, 171–190.

Treguier, A. M., I. M. Held, and V. D. Larichev, 1997: Parameterization of quasigeostrophic eddies in primitive equation ocean models. *J. Phys. Oceanogr.,* **27,** 567–580.

Veronis, G., 1975: The role of models in tracer studies. *Numerical Models of the Ocean Circulation,* Natl. Acad. Sci., 133–146.

Warren, B. A., 1976: Structure of deep western boundary currents. *Deep-Sea Res.,* **23,** 129–142.

——, 1981: Deep circulation of the world ocean. *Evolution of Physical Oceanography,* B. A. Warren and K. Wunsch, Eds., The MIT Press, 6–41.

Weaver, A. J., and M. Eby, 1997: On the numerical implementation of advection schemes for use in conjunction with various mixing parameterizations in the GFDL ocean model. *J. Phys. Oceanogr.,* **27,** 369–377.